

# We are IntechOpen, the world's leading publisher of Open Access books Built by scientists, for scientists

6,900

Open access books available

186,000

International authors and editors

200M

Downloads

Our authors are among the

154

Countries delivered to

TOP 1%

most cited scientists

12.2%

Contributors from top 500 universities



WEB OF SCIENCE™

Selection of our books indexed in the Book Citation Index  
in Web of Science™ Core Collection (BKCI)

Interested in publishing with us?  
Contact [book.department@intechopen.com](mailto:book.department@intechopen.com)

Numbers displayed above are based on latest data collected.  
For more information visit [www.intechopen.com](http://www.intechopen.com)



# Shear Mode Piezoelectric Thin Film Resonators

Takahiko Yanagitani  
Nagoya Institute of Technology  
Japan

## 1. Introduction

### 1.1 Shear mode bulk acoustic wave devices and sensors

Acoustic microsensor technique, well known as QCM (Quartz crystal microbalance) or TSM (Thickness shear mode) sensor, is an effective method to detect small mass loading on the sensor surface. This sensor can be operated even in liquid by using shear mode resonance. Therefore, shear mode piezoelectric film resonators are attractive for liquid microsensor technique such as biosensors and immunosensors.

Shear wave has some unique features compared with the longitudinal wave, for example, it has extremely low velocity in the liquid. Longitudinal wave velocity in the water is 1492.6 m/s, whereas, shear wave velocity in the water is 20-60 m/s at 20-200 MHz (Matsumoto et al., 2000). Therefore, shear mode vibrating solid maintains its vibration even in the liquid, because the difference of acoustic impedance which determines the reflection coefficient of solid / liquid interface is very large in the case of shear wave.

The complex reflection coefficient  $\Gamma$  of the interface is given as

$$\Gamma = \frac{Z_l - Z_s}{Z_l + Z_s} \quad (1)$$

where  $Z_s$  and  $Z_l$  are the complex acoustic impedance of solid and liquid.

Complex acoustic impedance can be written as

$$Z = R + jX = (\rho(c + j\omega\eta))^{1/2} \quad (2)$$

$R$  and  $X$  represent the real part and imaginary part of the acoustic impedance and  $\rho$ ,  $c$  and  $\eta$  represent mass density, stiffness constant and viscosity in the medium, respectively.

Acoustic wave equation gives dispersion relation of

$$\left(\frac{\omega}{v} - j\alpha\right)^2 (c + j\omega\eta) = \rho\omega^2 \quad (3)$$

where  $v$  is velocity and  $\alpha$  is attenuation factor (B. A. Auld, 1973).

According to (2) and (3), acoustic impedance gives

$$R = \frac{\rho v \omega^2}{\omega^2 + \alpha^2 v^2}, \quad X = \frac{\rho v^2 \omega \alpha}{\omega^2 + \alpha^2 v^2} \quad (4)$$

Longitudinal and shear wave velocities of water were reported as 1492.6 m/s (Kushibiki et al., 1995) and 35 m/s (Matsumoto et al., 2000), respectively, at 100 MHz. Attenuations of longitudinal and shear wave in the water were also measured to be  $\alpha/f^2 = 2.26 \times 10^{-14}$  neper s<sup>2</sup>/m (Kushibiki et al., 1995) and  $\alpha/f^2 = 2.12 \times 10^{-9}$  neper s<sup>2</sup>/m, (Matsumoto et al., 2000) respectively. By substituting these values into Eq. (4), the complex longitudinal wave and shear wave acoustic impedance of the water can be estimated to be  $1489000 + j800$  N s/m<sup>3</sup> and  $14510 + j17340$  N s/m<sup>3</sup> at 100 MHz, respectively.

From these values and Eq. (1), when quartz resonator is immersed in water, the reflection coefficient of acoustic energy  $|\Gamma|^2$  in an X-cut quartz vibrating in thickness extensional mode ( $Z_s = 15.23 \times 10^{-6}$  N s/m<sup>3</sup>) is estimated to be only 68 % whereas that in an AT-cut quartz vibrating in thickness shear mode ( $Z_s = 8.795 \times 10^{-6}$  N s/m<sup>3</sup>) is 98 %. This is because an AT-cut quartz has been used as a QCM or TSM sensor operating in liquid. Sensitivity of the QCM mass sensor is determined by the ratio of the mass and the entire mass of the vibrating part in the sensor, at constant sensor active area (Sauerbrey, 1959). Therefore, it is important to decrease thickness of the vibrating part of sensor. Shear mode thin film is promising for high sensitivity mass sensor.

### 1.2 Piezoelectric thin film for shear mode excitation

Piezoelectric thin film, which excites shear wave, is expected to provide higher sensitivity and IC compatibility, but it is not straightforward. To excite shear wave by standard sandwiched electrode configuration, polarization axis in the film must be tilted or parallel to the film plane. Although perovskite ferroelectric films have large piezoelectricity, their polarization axis is generally normal to the film surface due to the nature of crystal growth, difficulty of in-plane polarization treatment and domain control. Trigonal piezoelectric material such as LiNbO<sub>3</sub>, LiTaO<sub>3</sub> and quartz are difficult to crystallize (tend to form amorphous structure) or to obtain a strong preferred orientation in polycrystalline film.

6mm wurtzite AlN and ZnO film can be easily crystallized, but they tend to develop their polarization axis (c-axis) perpendicular to the substrate plane. This c-axis oriented film cannot excite shear wave in the case of standard sandwiched electrode structure.

Crystalline orientation control for both in-plane and out-of-plane direction is necessary to excite shear wave. One solution is to use an epitaxial growth technique. However, the combinations of the shear mode piezoelectric film and substrate are limited due to the lattice mismatch. a-plane ZnO or AlN/r-plane sapphire (Mitsuyu et al., 1980; Wittstruck et al., 2003), a-plane ZnO/42° Y-X LiTaO<sub>3</sub> (Nakamura et al., 2000) where c-axis in the film is parallel to the substrate plane have been reported.

Ion beam orientation control technique (Yanagitani & Kiuchi, 2007c), which enables in-plane and out-of-plane orientation without use of epitaxial growth, is introduced in the third section. This technique is a good candidate for obtaining c-axis parallel films which excites pure shear wave without any excitation of longitudinal wave.

## 2. Electromechanical coupling properties of wurtzite crystal

Elastic and piezoelectric properties of wurtzite crystals vary with direction due to the crystal anisotropy. Electromechanical coupling changes as a function of the angle between the c-axis and the applied electric field direction (Foster et al., 1968; Auld, 1973).

The analytical model of a thin film resonator is shown in Fig. 1. The electric field is applied in the  $x_3$  direction. The c-axis is assumed to lie in the  $x_1$ - $x_3$  plane and be inclined at an angle  $\beta$  with respect to the  $x_3$  direction.

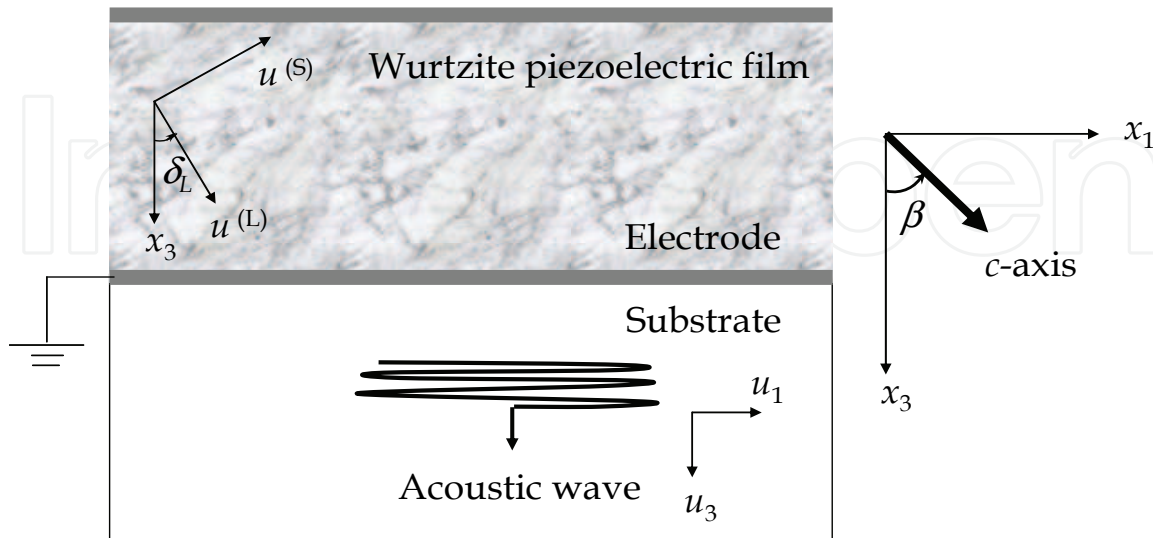


Fig. 1. Analytical model of a thin film resonator

The physical constants of the crystal in each direction are determined by the transformed coordinate of each constant tensor. Bond’s method (Bond, 1943) for transforming the elastic and piezoelectric constant tensor is introduced below, which can be applied to the constant tensor with abbreviated subscript notation. For example, the transformation matrix  $[a]$  of a clockwise rotation through an angle  $\beta$  about the  $x_2$ -axis is described by:

$$[a] = \begin{bmatrix} \cos \beta & 0 & -\sin \beta \\ 0 & 1 & 0 \\ \sin \beta & 0 & \cos \beta \end{bmatrix} \tag{5}$$

The dielectric constant  $\epsilon'$  transforms as

$$[\epsilon'] = [a] [\epsilon] [a]^T \tag{6}$$

The 6×6 transformation matrix of coefficients  $M$  is defined as

$$[M] = \begin{bmatrix} a_{xx}^2 & a_{xy}^2 & a_{xz}^2 & 2a_{xy}a_{xz} & 2a_{xz}a_{xx} & 2a_{xx}a_{xy} \\ a_{yx}^2 & a_{yy}^2 & a_{yz}^2 & 2a_{yy}a_{yz} & 2a_{yz}a_{yx} & 2a_{yx}a_{yy} \\ a_{zx}^2 & a_{zy}^2 & a_{zz}^2 & 2a_{zy}a_{zz} & 2a_{zz}a_{zx} & 2a_{zx}a_{zy} \\ a_{yx}a_{zx} & a_{yy}a_{zy} & a_{yz}a_{zz} & a_{yy}a_{zz} + a_{yz}a_{zy} & a_{yx}a_{zz} + a_{yz}a_{zx} & a_{yy}a_{zx} + a_{yx}a_{zy} \\ a_{zx}a_{xx} & a_{zy}a_{xy} & a_{zz}a_{xz} & a_{xy}a_{zz} + a_{xz}a_{zy} & a_{xz}a_{zx} + a_{xx}a_{zz} & a_{xx}a_{zy} + a_{xy}a_{zx} \\ a_{xx}a_{yx} & a_{xy}a_{yy} & a_{xz}a_{yz} & a_{xy}a_{yz} + a_{xz}a_{yy} & a_{xz}a_{yx} + a_{xx}a_{yz} & a_{xx}a_{yy} + a_{xy}a_{yx} \end{bmatrix} \tag{7}$$

Finally, using the above transformation matrix, transformed elastic constant and piezoelectric constant tensors  $c'$  and  $e'$  are obtained:

$$[c'] = [M] [c] [M]^T, [e'] = [M] [e] [M]^T \quad (8)$$

In the  $x_2$  axis rotation of a hexagonal (6mm) crystal, the transformed stiffness and piezoelectric constant tensors  $c'$  and  $e'$  are given by

$$[c'] = \begin{bmatrix} c'_{11} & c'_{12} & c'_{13} & 0 & c'_{15} & 0 \\ c'_{12} & c'_{22} & c'_{23} & 0 & c'_{25} & 0 \\ c'_{13} & c'_{23} & c'_{33} & 0 & c'_{35} & 0 \\ 0 & 0 & 0 & c'_{44} & 0 & c'_{46} \\ c'_{15} & c'_{25} & c'_{35} & 0 & c'_{55} & 0 \\ 0 & 0 & 0 & c'_{46} & 0 & c'_{66} \end{bmatrix}, [e'] = \begin{bmatrix} e'_{11} & e'_{12} & e'_{13} & 0 & e'_{15} & 0 \\ 0 & 0 & 0 & e'_{24} & 0 & e'_{26} \\ e'_{31} & e'_{32} & e'_{33} & 0 & e'_{35} & 0 \end{bmatrix} \quad (9)$$

In case, wave propagation toward  $x_3$  direction is only focused, the term of  $\partial/\partial x_1$  and  $\partial/\partial x_2$  can be ignored. Thus, the wave motion equation for the  $x_3$  direction is given by mechanical displacement component  $u_1, u_2$  and  $u_3$ :

$$\frac{\partial T_{31}}{\partial x_3} = \rho \frac{\partial^2 u_1}{\partial t^2} \quad (10a)$$

$$\frac{\partial T_{33}}{\partial x_3} = \rho \frac{\partial^2 u_3}{\partial t^2} \quad (10b)$$

$$\frac{\partial T_{32}}{\partial x_3} = \rho \frac{\partial^2 u_2}{\partial t^2} \quad (10c)$$

where

$$T_{31} = c'_{55} \frac{\partial u_1}{\partial x_3} + c'_{35} \frac{\partial u_3}{\partial x_3} + e'_{35} \frac{\partial \varphi}{\partial x_3} \quad (11a)$$

$$T_{33} = c'_{35} \frac{\partial u_1}{\partial x_3} + c'_{33} \frac{\partial u_3}{\partial x_3} + e'_{33} \frac{\partial \varphi}{\partial x_3} \quad (11b)$$

$$T_{32} = c'_{44} \frac{\partial u_2}{\partial x_3} \quad (11c)$$

As  $\text{div } D = 0$ , the electrostatic equation is given by

$$\frac{\partial D_3}{\partial x_3} = e'_{35} \frac{\partial^2 u_1}{\partial x_3^2} + e'_{33} \frac{\partial^2 u_3}{\partial x_3^2} - \epsilon'_{33} \frac{\partial^2 \varphi}{\partial x_3^2} = 0 \quad (12)$$

In Eqs. (10)-(12),  $T_{31}$  and  $T_{33}$  are stress components,  $D_3$  is the electric displacement,  $c_{33}^E$ ,  $c_{35}^E$  and  $c_{55}^E$  are the stiffness constants with constant electric field,  $e_{33}$  and  $e_{35}$  are piezoelectric constants,  $\epsilon_{33}^S$  and  $\epsilon_{35}^S$  are dielectric constants with constant strain, and  $\varphi$  is the electric potential.

Equation (10c) describes a pure shear wave with a  $u_2$  displacement component in the  $x_2$  direction and propagates along the  $x_3$  direction with a phase velocity of  $\sqrt{c_{44}/\rho}$ . Eqs. (10a) and (10b) represent a quasi-longitudinal wave and quasi-shear wave. These waves incorporate  $u_1$ ,  $u_3$ , and  $\varphi$ , which are coupled with each other. It is well known that Eqs (10a), and (10b) have plane-wave solutions:

$$\begin{pmatrix} u_1 \\ u_3 \\ \varphi \end{pmatrix} = \begin{pmatrix} A \\ B \\ C \end{pmatrix} \exp \left\{ j\omega \left( t - \frac{x_3}{v} \right) \right\} \quad (13)$$

Substituting Eq. (13) into Eqs. (11) and (12), the simultaneous equations are obtained

$$\begin{pmatrix} c_{55}^D - \rho v^2 & c_{35}^D & 0 \\ \bar{c}_{35} & c_{33}^D - \rho v^2 & 0 \\ -e_{35} & -e_{33} & \epsilon_{33}^S \end{pmatrix} \begin{pmatrix} A \\ B \\ C \end{pmatrix} = 0, \quad (14)$$

where

$$\begin{aligned} c_{33}^D &= c_{33}^E + (e'_{33})^2 / \epsilon_{33}^S, \\ c_{35}^D &= c_{35}^E + (e'_{33} e'_{35}) / \epsilon_{33}^S, \\ c_{55}^D &= c_{55}^E + (e'_{35})^2 / \epsilon_{33}^S. \end{aligned} \quad (15)$$

A, B and C are all nonzero when the coefficient matrix in Eq. (14) is zero. From this condition, we obtain the phase velocity  $v^{(L,S)}$  of a quasi-longitudinal wave and quasi-shear wave:

$$v^{(L,S)} = \left[ \frac{c_{33}^D + c_{55}^D}{2\rho} \pm \sqrt{\left( \frac{c_{33}^D - c_{55}^D}{2\rho} \right)^2 + \left( \frac{c_{35}^D}{\rho} \right)^2} \right]^{\frac{1}{2}} \quad (16)$$

Figure 2 shows the calculated results of phase velocity of a quasi-longitudinal wave and quasi-shear wave for a ZnO crystal as function of the angle  $\beta$  between the c-axis and  $x_3$  direction. Physical constants in a ZnO single crystal reported by Smith were used in the calculation (Smith, 1969).

The general solutions for  $u_1$ ,  $u_3$  and  $\varphi$  are given by

$$\begin{pmatrix} u_1 \\ u_3 \\ \varphi \end{pmatrix} = \begin{pmatrix} A_1 \\ B_1 \\ C_1 \end{pmatrix} \exp \left\{ j\omega \left( t - \frac{x_3}{V^{(+)}} \right) \right\} + \begin{pmatrix} A_2 \\ B_2 \\ C_2 \end{pmatrix} \exp \left\{ j\omega \left( t - \frac{x_3}{V^{(-)}} \right) \right\} \quad (17)$$

and

$$\frac{B_1}{A_1} = -\frac{A_2}{B_2} \quad (18)$$

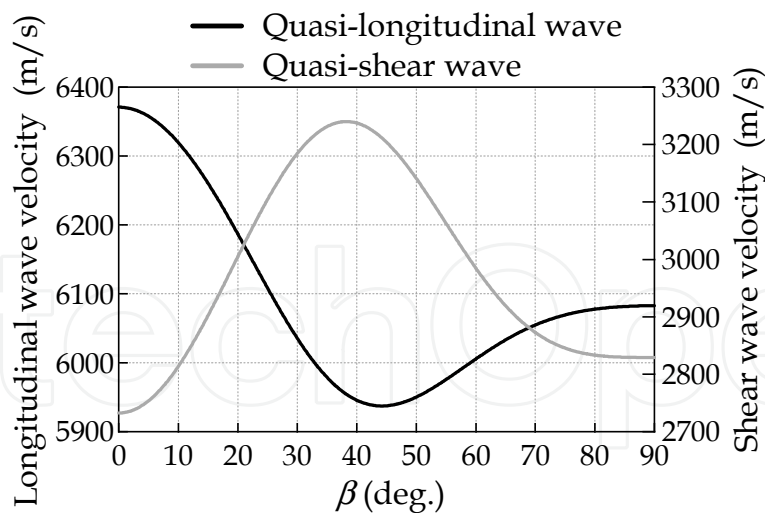


Fig. 2. Phase velocity of quasi-longitudinal wave and quasi-shear wave for a ZnO crystal as function of the angle  $\beta$  between the c-axis and  $x_3$  direction

is derived from Eqs. (14) and (16). It can be seen that the displacement components of the quasi-longitudinal wave and quasi-shear wave are perpendicular to each other. From Eqs. (14) and (16), the angle  $\delta_L$  between the quasi-longitudinal wave displacement  $u_3$  and the  $x_3$  direction and the angle  $\delta_S$  between the quasi-shear wave displacement  $u_1$  and the  $x_1$  direction are given by

$$\delta_L = \tan^{-1}\left(\frac{A_1}{B_1}\right), \quad \delta_S = \tan^{-1}\left(\frac{B_2}{A_2}\right) \quad (19)$$

The extensional and shear effective piezoelectric constants  $e^{(L)}_{eff}$  and  $e^{(S)}_{eff}$  are defined as

$$e^{(L)}_{eff} = e'_{35} \sin \delta_L + e'_{33} \cos \delta_L, \quad e^{(S)}_{eff} = e'_{35} \cos \delta_S - e'_{33} \sin \delta_S \quad (20)$$

Thus, the quasi-longitudinal and quasi-shear-mode electromechanical coupling coefficients  $k^{(L)}$  (transformed  $k_{33}$ ) and  $k^{(S)}$  (transformed  $k_{15}$ ) are

$$\left(k^{(S)}\right)^2 = \left(e^{(S)}\right)^2 / e'_{33} \rho \left(V^{(-)}\right)^2, \quad \left(k^{(L)}\right)^2 = \left(e^{(L)}\right)^2 / e'_{33} \rho \left(V^{(+)}\right)^2 \quad (21).$$

Finally, Figs. 3 (a) and (b) show the calculated angle  $\delta$  and the electromechanical coupling coefficients ( $k$  values) of the quasi-longitudinal and quasi-shear waves for the ZnO crystal as function of the angle  $\beta$  (Foster et al., 1968)

From these figures, we can see a relatively large shear-mode electromechanical coupling  $k_{15} = 0.39$  at c-axis tilt angle of  $\beta = 28^\circ$ . Several author reported FBAR (film bulk acoustic resonator)-type viscosity sensor and biosensor, consisting of c-axis tilted wurtzite films (Weber et al., 2006; Link et al., 2007; Wingqvist et al., 2007, 2009, 2010; Yanagitani, 2010, 2011a). However, the thickness extensional mode (longitudinal wave mode) also has the coupling of  $k_{33} = 0.155$  and the displacement inclination angle of  $\delta_S = 4.1^\circ$  at angle of  $\beta = 28^\circ$ . This indicates that the resonator excites both thickness extensional and shear mode (longitudinal and shear wave modes), and the shear displacement direction is not perpendicular to the propagation direction. Larger  $\delta_S$  values may result in energy leakage

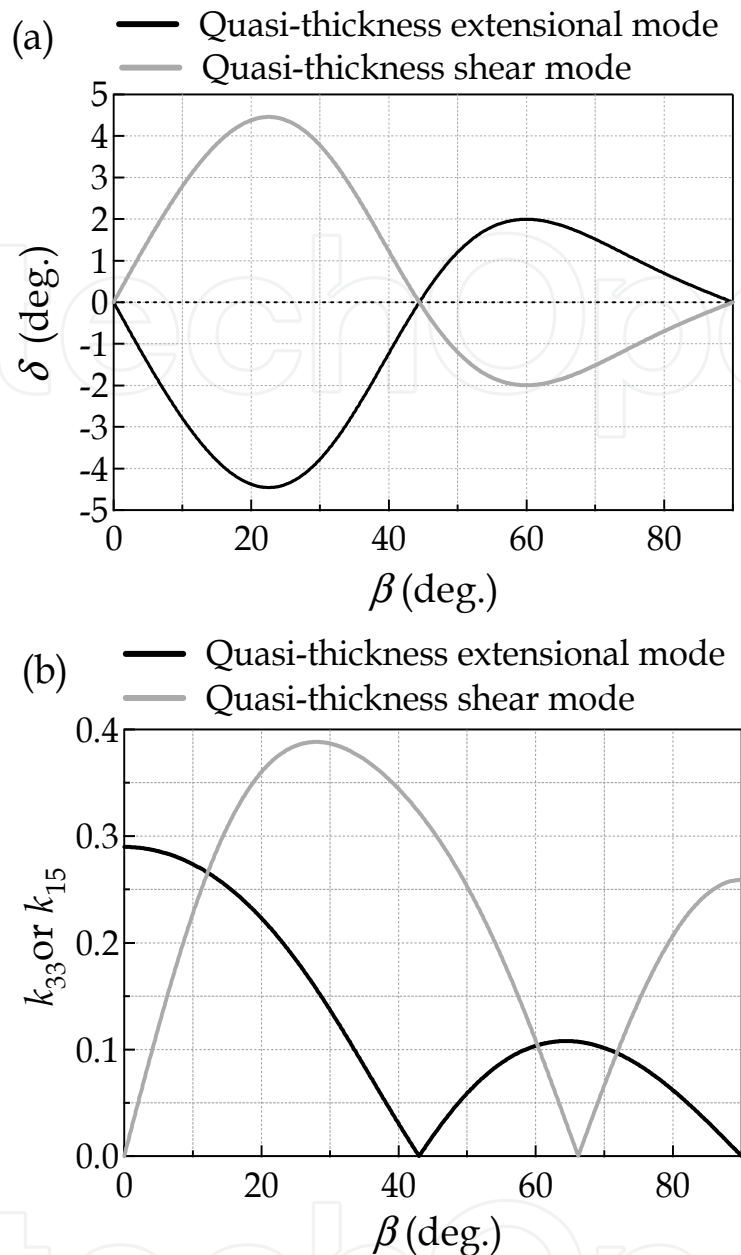


Fig. 3. (a) Angle  $\delta$  between the wave displacement  $u$  and the  $x$  direction and (b) electromechanical coupling coefficient of the quasi-longitudinal and quasi-shear waves for the ZnO crystal as function of the angle  $\beta$  between the  $c$ -axis and  $x_3$  direction

due to mode conversion in the reflection plane. This induces the decrease of  $Q$  value. Both of the no extensional mode coupling and small  $\delta_s$  values of  $0.38^\circ$  can be obtained at  $\beta = 43^\circ$ , however, it is difficult to adjust such as large  $c$ -axis tilt angle in a large area deposition. One option is to use a pure-shear-mode ( $\beta = 90^\circ$ ) resonator to satisfy both the conditions of no extensional coupling and  $\delta_s = 0^\circ$ . Pure shear mode excitation can be achieved by two electric field-orientation combination. One is to apply the cross-electric field to  $c$ -axis parallel film by sandwiched electrode (Yanagitani et al., 2007d), and the other is to apply the in-plane electric field to  $c$ -axis normal film by IDT electrode (Corso et al., 2007; Milyutin et al., 2008, 2010). Of course, the latter is the easiest way to obtain pure shear mode because deposition

technique of c-axis normal film has been well established, but effective electrometrical coupling is weak ( $k_{eff}=0.04-0.06$ ) (Corso et al., 2007; Milyutin et al., 2008). The former has large electrometrical coupling ( $k_{15}=0.24$ ) (Yanagitani et al., 2007a), and recently the c-axis parallel oriented film can be easily obtained by using ion beam orientation control technique (presented in next section), even in a large area (Kawamoto et al., 2010).

### 3. Ion beam orientation control technique for shear mode piezoelectric films

#### 3.1 Ion beam orientation control of wurtzite thin film by ion beam irradiation

Polycrystalline films tend to grow in their most densely packed plane parallel to the substrate plane. Bravais proposed the empirical rule that the growth rate of the crystal plane is proportional to the surface atomic density. Namely, the lattice plane with higher surface atomic density grows more rapidly. Curie argued that the growth rate perpendicular to a plane is proportional to the surface free energy (Curie, 1885).

Ion bombardment during film deposition can modify this preferred orientation of the films. This is usually explained by a change in anisotropy of the growing rate of the crystal plane in the grain, which is reflected by the difference in the degree of the ion channeling effect or ion-induced damage in the crystal plane (Bradley et al., 1986; Ensinger, 1995; Ressler et al., 1997; Dong & Srolovitz, 1999). For example, during ion beam irradiation, the commonly observed  $\langle 111 \rangle$  preferred orientation in a face-centered cubic film changes to a  $\langle 110 \rangle$  preferred orientation, which corresponds to the easiest channeling direction (Van Wyk & Smith, 1980; Dobrev, 1982). In-plane texture controls have also been achieved by optimizing the incident angle of the ion beam (Yu et al., 1985; Iijima et al., 1992; Harper et al., 1997; Kaufman et al., 1999; Dong et al., 2001; Park et al., 2005).

In wurtzite films, for example, the surface energy densities of the (0001),  $(11\bar{2}0)$  and  $(10\bar{1}0)$  planes of the ZnO crystal are estimated to be 9.9, 12.3, 20.9 eV/nm<sup>2</sup>, respectively (Fujimura et al., 1993). The (0001) plane has the lowest surface density. Thus, the ZnO film tends to grow along the [0001] direction. When wurtzite crystal is irradiated with ion beam, the most densely packed (0001) plane should incur more damage than the  $(10\bar{1}0)$  and  $(11\bar{2}0)$  planes, which correspond to channeling directions toward the ion beam irradiation. We can therefore expect that the thermodynamically preferred (0001) oriented grain growth will be disturbed by ion damage so that the damage-tolerant  $(10\bar{1}0)$  or  $(11\bar{2}0)$  orientated grains (c-axis parallel oriented grain) will preferentially develop instead.

On this basis, in-plane and out-of-plane orientation control of AlN and ZnO films by means of ion beam-assisted deposition technique, such as evaporation (Yanagitani & Kiuchi, 2007c) and sputtering (Yanagitani & Kiuchi, 2007e, 2011b) was achieved. c-axis parallel oriented can be obtained even in a conventional magnetron sputtering technique using a low pressure discharge ( $<0.1$  Pa) (Yanagitani et al., 2005) or RF substrate bias (Takayanagi, 2011), which leads ion bombardment on the substrate. Figure 4 shows the XRD patterns of the ZnO films deposited with various ion energy and amount of flux in ion beam assisted evaporation (Yanagitani & Kiuchi, 2007c). Table 1 shows the ion current densities in the case of "Large ion flux" and "Small ion flux" in Fig 4. The tendency of the  $(10\bar{1}0)$  orientation is enhanced with increasing ion energy and amount of ion irradiation, demonstrating that the ion bombardment induced the (0001) orientation to change into a  $(10\bar{1}0)$  orientation, which corresponds to the ion channeling direction.

Ion energy	A: Large ion flux	B: Small ion flux
0.05 keV	0-5 $\mu\text{A}/\text{cm}^2$	
0.25 keV	30-50 $\mu\text{A}/\text{cm}^2$	
0.5 keV	190 $\mu\text{A}/\text{cm}^2$	140 $\mu\text{A}/\text{cm}^2$
0.75 keV	220 $\mu\text{A}/\text{cm}^2$	130 $\mu\text{A}/\text{cm}^2$
1.0 keV	240 $\mu\text{A}/\text{cm}^2$	120 $\mu\text{A}/\text{cm}^2$

Table 1. Ion current densities in “Large ion flux” and “Small ion flux”

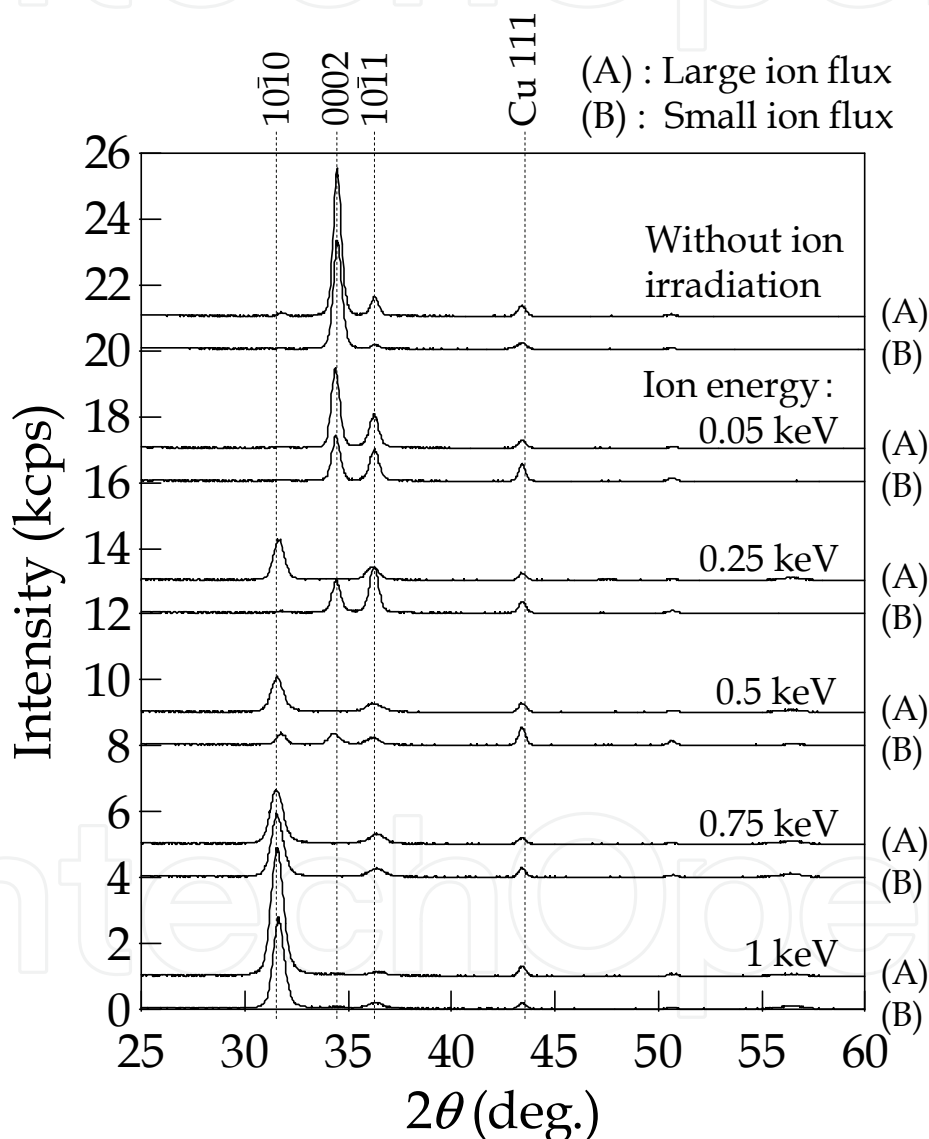


Fig. 4.  $2\theta-\omega$  scan XRD patterns of the ZnO films deposited without ion irradiation, and with ion irradiation of 0-1 keV with “Large ion flux” and “Small ion flux” (Yanagitani & Kiuchi, 2007c)

Figure 5 shows the XRD patterns of the samples deposited under the conditions that various RF and DC bias are applied to the substrate. Although any dramatic change in usual (0001)

preferred orientation is not occurred in the case of positive or negative DC bias, (0001) orientation changed to  $(11\bar{2}0)$  and  $(10\bar{1}0)$  orientation with the increase of RF bias power which induces the bombardment of positive ion on substrate. Interestingly, the order of the appearance of the (0001) to  $(11\bar{2}0)$  and  $(10\bar{1}0)$  corresponds to the order of increasing surface atomic density, which may be the order of damage tolerance against ion bombardment.

In order to excite shear wave in the c-axis parallel film, c-axis is required to orient not only in out-of-plane direction but also in in-plane direction. The ion beam orientation control technique allows us to control even in in-plane c-axis direction and polarization by the direction of beam incident direction (Yanagitani et al., 2007d).

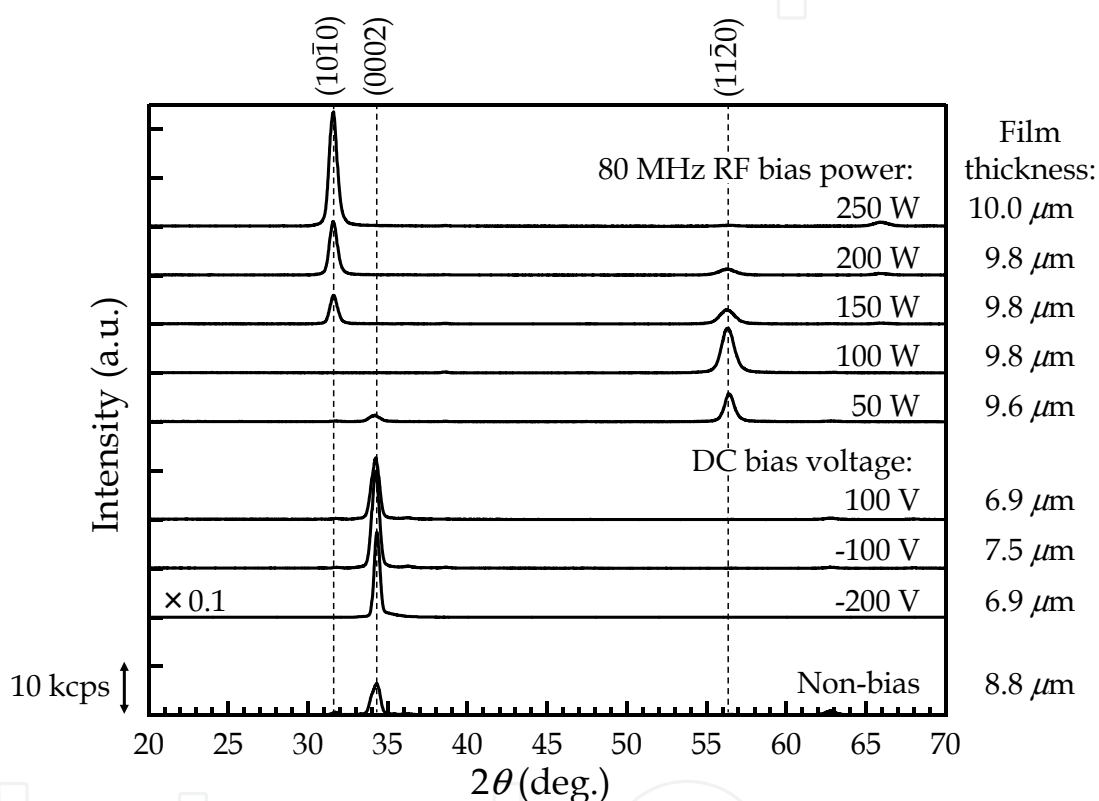


Fig. 5.  $2\theta$ - $\omega$  scan XRD patterns of the samples deposited without bias, with 80 MHz RF bias of 50 to 250 W, or with -200 to 100 DC bias. All samples were measured at the center of the bias electrode (Takayanagi et al., 2011)

#### 4. Method for determining $k$ values in piezoelectric thin films

##### 4.1 $k$ value determination using as-deposited structure (HBAR structure)

A method for determining piezoelectric property in thin films is described in this section. In general, electromechanical coupling coefficient ( $k$  value) in thin film can be easily determined by series and parallel resonant frequency of a FBAR consisting of top electrode layer/piezoelectric layer/bottom electrode layer or SMR (Solidly mounted resonator) consisting of top electrode layer/piezoelectric layer/bottom electrode layer/Bragg reflector. In case thickness of electrode film is negligible small compared with that of piezoelectric film,  $k$  of the piezoelectric film can be written as follows (Meeker, 1996):

$$k^2 = \frac{\pi f_s}{2 f_p} \tan\left(\frac{\pi f_p - f_s}{2 f_p}\right) \quad (22)$$

where  $f_p$  and  $f_s$  are the parallel resonant frequency and series resonant frequency, respectively.

However, it takes considerable time and effort to fabricate FBAR structure which have self-standing piezoelectric layer. It is convenient if  $k$  value can be determined from as deposited structure, namely so-called an HBAR (high-overtone bulk acoustic resonator) or composite resonator structure consisting of top electrode layer/piezoelectric layer/bottom electrode layer/thick substrate. Methods for determining the  $k$  value of the films from HBAR structure are more complex than that for the self-supported single piezoelectric film structure (FBAR structure). Several groups have investigated methods for the determination of  $k_t$  value from the HBAR structure (Hickernell, 1996; Naik, et al., 1998; Zhang et al., 2003). One of the easiest ways of  $k$  determination is to use a conversion loss characteristic of the HBAR structure. When the thickness of electrode layers is negligible small compared with that of piezoelectric layer, capacitive impedance of resonator is equal to the electrical source impedance, and  $k$  value of the piezoelectric layer is smaller than 0.3, conversion loss  $CL$  is approximately represented by  $k$  value at parallel resonant frequency (Foster et al., 1968):

$$CL \approx 10 \log_{10} \frac{\pi}{8k^2} \cdot \frac{Z_s}{Z_p} \quad (23)$$

where,  $Z_s$  and  $Z_p$  is acoustic impedance of the substrate and piezoelectric layer, respectively. However, various inhomogeneities sometimes exist in the film resonator, such as non-negligible thick and heavy electrode layers, thickness taper, or the piezoelectrically inactive layer composed of randomly oriented grains growing in the initial stages of the deposition. In this case, the  $k$  values of the film can be determined so as to match the experimentally measured conversion losses ( $CL$ ) of the resonators with theoretical minimum  $CL$  by taking  $k$  value as adjustable parameter. The theoretical  $CL$  in this case can be calculated by Mason's equivalent circuit model including electrode layer, film thickness taper and piezoelectrically inactive layer. This method allows various inhomogeneous effect of film to be taken into account (Yanagitani et al., 2007b, 2007c).

#### 4.2 Experimental method to estimate conversion loss of HBAR structure

The experimental  $CL$  of HBAR can be determined from reflection coefficients ( $S_{11}$ ) of the resonators, which can be obtained using a network analyzer with a microwave probe. The inverse Fourier transform of  $S_{11}$  frequency response of the resonator gives the impulse response of the resonator in the time domain. In the HBAR structure, the impulse response is expected to include echo pulse trains reflected from the bottom surface of the substrate, and the insertion loss of resonator can be obtained from the Fourier transform of the first echo in this impulse response. This experimental insertion loss  $IL_{\text{experiment}}$  includes doubled  $CL$  in the piezoelectric film and round-trip diffraction loss  $DL$  and round-trip propagation loss  $PL$  in the silica glass substrate. Therefore,  $CL$  can be expressed as

$$CL = \frac{1}{2} ( IL_{\text{experiment}} - DL - PL ), \quad (24)$$

where diffraction loss  $DL$  can be calculated according to the method reported by Ogi *et al.* (Ogi *et al.*, 1995). This method is based on integration of the velocity potential field in the divided small transducer elements, which allows calculation of the  $DL$  with electrode areas of various shapes. The round-trip propagation loss  $PL$  is given as

$$PL = 2d_s \frac{\alpha_s}{f^2}, \quad (25)$$

where  $d_s$  is the thickness of the substrate,  $\alpha_s$  represents the shear wave attenuation in the substrate, for example,  $\alpha_s / f^2 = 19.9 \times 10^{-16}$  (dB · s<sup>2</sup>/m) in silica glass substrate (Fraser, 1967).

#### 4.3 Conversion loss simulation in HBAR by Mason's equivalent circuit model

Electromechanical coupling coefficient  $k$  can be estimated by comparing an experimental  $CL$  with a theoretical  $CL$  of the HBAR. One-dimensional Mason's equivalent circuit model is convenient tool for simulating theoretical  $CL$  of the resonator. Generally, in case non-piezoelectric elastic solid vibrates in thickness mode, its can be described as T-type equivalent circuit (Fig. 6 (a)) where  $F_1$  and  $F_2$  are force and  $v_1$  and  $v_2$  are particle velocity acting on each surface of elastic solid. Piezoelectric elastic solid can be represented as the Mason's three ports equivalent circuit which includes additional electric terminal concerning electric voltage  $V$  and current  $I$  (Fig. 6 (b)) (Mason, 1964). Here,  $\gamma$  is propagation constant,  $Z$  is acoustic impedance and  $d_p$  is thickness of elastic solid. To take account of attenuation of vibration, mechanical quality factor  $Q_m$  is defined as  $Q_m = c_r / c_i$  where  $c_r$  and  $c_i$  are real part and imaginary part of elastic constant, respectively. Using mechanical quality factor  $Q_m$ , propagation constant  $\gamma$  and acoustic impedance  $Z$  are given as:

$$\gamma = j\omega \sqrt{\frac{\rho}{c_r \{ 1 + j (1/Q_m) \}}}, \quad Z = S \sqrt{\rho c_r \{ 1 + j (1/Q_m) \}} \quad (26)$$

where  $\rho$  is density of the elastic solid and  $S$  is electrode area of the resonator. Static capacitance  $C_0$  and ratio of transformer  $\phi_0$  in the circuit are given as:

$$C_0 = \epsilon_{11}^s \frac{S}{d_p}, \quad \phi_0 = \left[ \frac{C_0 v_p Z_p \left( \frac{k_{15}^2}{1 - k_{15}^2} \right)}{d_p} \right]^{\frac{1}{2}}, \quad (27),$$

where  $d$  is the thickness of the layers,  $\epsilon_{11}^s$  is permittivity, and  $v$  is the velocity of the shear wave. Subscript  $p$ ,  $e1$ ,  $e2$  and  $s$  respectively represent piezoelectric layer, top electrode layer, bottom electrode layer and substrate.  $k$  value affects the equivalent circuit through the ratio of transformer  $\phi_0$ .

Equivalent circuit for the over-moded resonator structure is given in Fig. 7 by cascade arranging non-piezoelectric and piezoelectric part as described in Figs. 6 (a) and (b). Substrate thickness is assumed infinite to ignore reflection waves from bottom surface of the substrate in this case. When the surface of the top electrode is stress-free, the acoustic input port is shorted. As top electrode part circuit can be simplified, three-port circuit in Fig. 7 is transformed to the two-ports circuit shown in Fig. 8 (Rosenbaum, 1988).

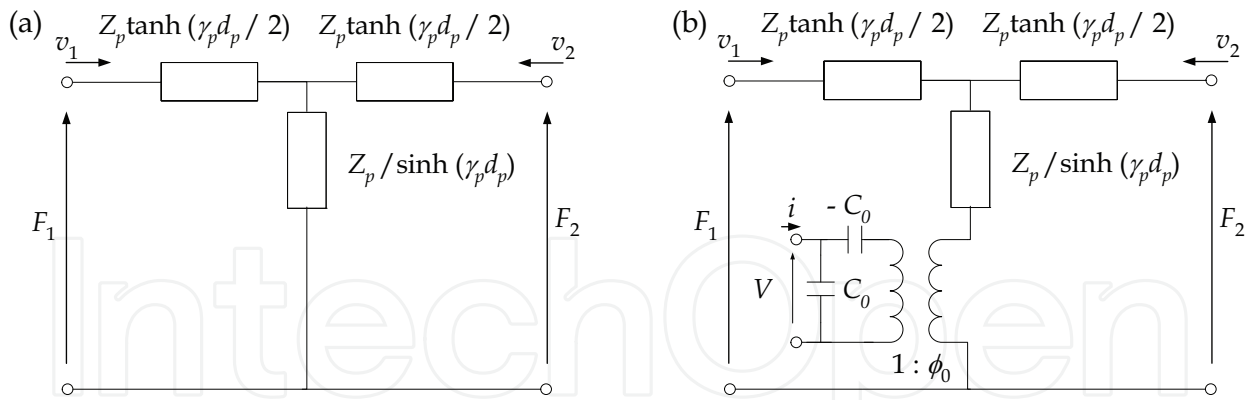


Fig. 6. Equivalent circuit model of (a) non-piezoelectric (b) piezoelectric elastic solid

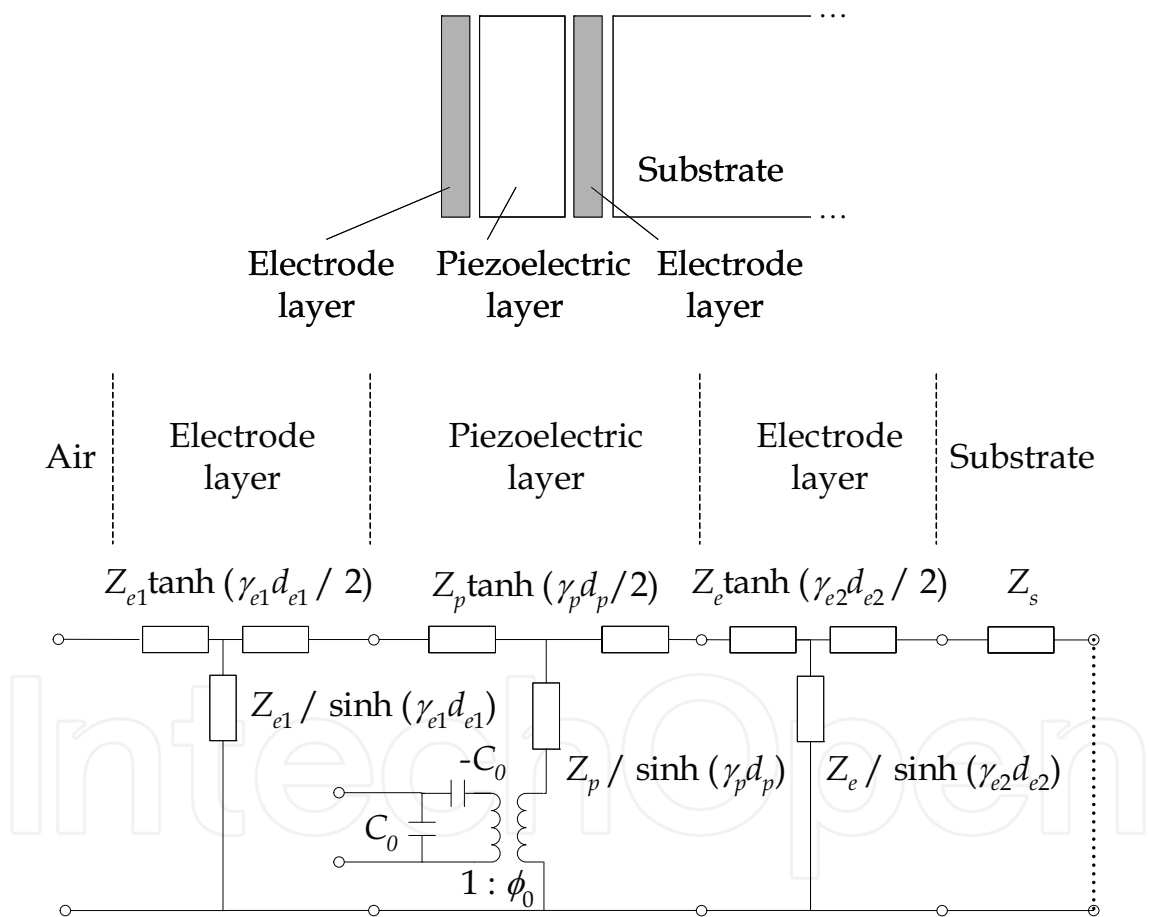


Fig. 7. Equivalent circuit model of the over-moded resonator structure

It is convenient to derive whole impedance of the circuit by using *ABCD*-parameters (Paco et al., 2008) As shown in Eqs. (28)-(32), *ABCD*-parameters of whole circuit is derived multiplying each circuit element.

$$F_{Transformer} = \begin{bmatrix} 1/\phi_0 & 0 \\ 0 & \phi_0 \end{bmatrix}, F_{Electric\ port} = \begin{bmatrix} 1 & 0 \\ j\omega C_0 & 1 \end{bmatrix}, F_{Substrate} = \begin{bmatrix} 1 & Z_s \\ 0 & 1 \end{bmatrix} \quad (28)$$

$$F_{Piezo+Electrode\ layer} = \begin{bmatrix} 1 & Z_p / \sinh(\gamma_p d_p) \\ 0 & 1 \end{bmatrix} \cdot \begin{bmatrix} 1 & 0 \\ 1 / \{ Z_{e1} \tanh(\gamma_{e1} d_{e1} / 2) + Z_p \tanh(\gamma_p d_p / 2) \} & 1 \end{bmatrix} \cdot \begin{bmatrix} 1 & Z_p \tanh(\gamma_p d_p / 2) \\ 0 & 1 \end{bmatrix} \quad (29)$$

$$F_{Counter-electrode} = \begin{bmatrix} 1 & Z_{e2} \tanh(\gamma_{e2} d_{e2} / 2) \\ 0 & 1 \end{bmatrix} \cdot \begin{bmatrix} 1 & 0 \\ \sinh(\gamma_{e2} d_{e2}) / Z_{e2} & 1 \end{bmatrix} \cdot \begin{bmatrix} 1 & Z_{e2} \tanh(\gamma_{e2} d_{e2} / 2) \\ 0 & 1 \end{bmatrix} \quad (30)$$

$$F_{Substrate} = \begin{bmatrix} 1 & Z_s \\ 0 & 1 \end{bmatrix} \quad (31)$$

$$F_{Over-moded\ resonator} = F_{Electric\ port} \cdot F_{Transformer} \cdot F_{Piezo+Electrode\ layer} \cdot F_{Counterelectrode} \cdot F_{Substrate} \quad (32)$$

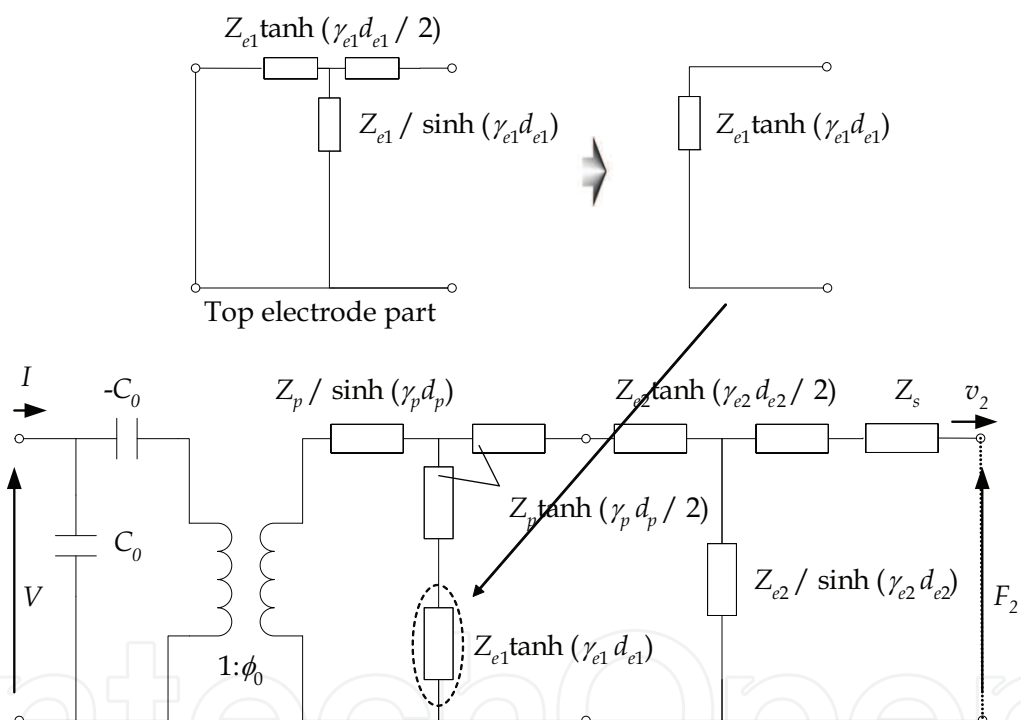


Fig. 8. Simplification of equivalent circuit model for over-moded resonator structure

Insertion loss  $IL$  is expressed as the ratio of the signal power delivered from a source into load resistance to the power delivered from a source into the inserted network.  $IL$  of the resonators can be calculated with the following equation using conductance of the electrical source  $G_s$  (0.02 S), input conductance  $G_f$ , and susceptance  $B_f$  of the circuit model, which can be derived from  $ABCD$ -parameter to  $Y$ -parameter conversion of eq. (32):

$$IL = 20 \log_{10} \frac{\Re \left\{ (G_f + jB_f) \frac{G_s^2}{(G_s + G_f)^2 + B_f^2} \right\}}{G_s/4} \quad (33)$$

Hence the  $CL$  is

$$CL = \frac{IL}{2} = 10 \log_{10} \frac{4G_s G_f}{(G_s + G_f)^2 + B_f^2} \tag{34}$$

**4.4  $k$  value determination from conversion loss curves**

Figure 9 (a) shows the pure shear mode theoretical and experimental  $CL$  curves of the c-axis parallel film HBAR as an example. By comparing experimental curve with theoretical curves

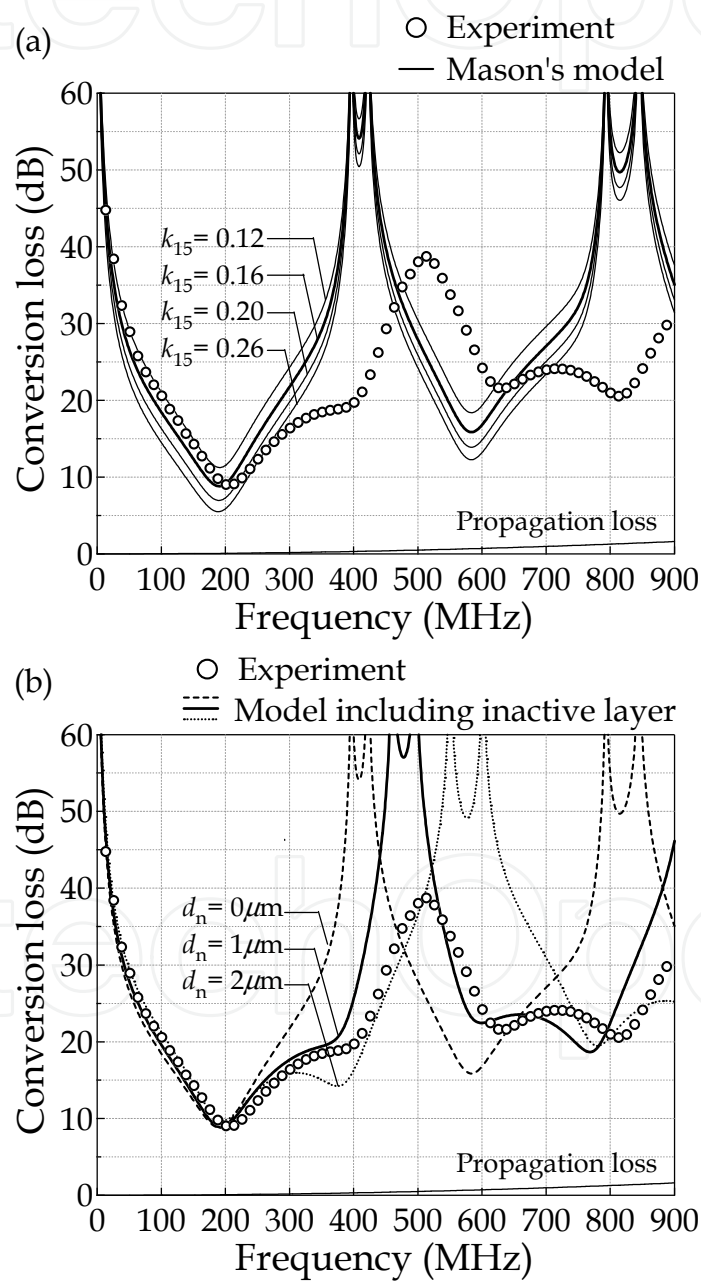


Fig. 9. Frequency response of the experimental shear mode  $CL$  (open circles). (a) The simulated shear mode  $CL$  curves (solid line) in various  $k_{15}$  values and (b) the curve simulated by the model including various thickness of piezoelectrically inactive layer (Yanagitani & Kiuchi, 2007c)

at minimum  $CL$  point (near the parallel resonant frequency), we can determine the  $k_{15}$  value of the film. As shown in Fig. 9 (b), effective thickness of the piezoelectrically inactive layer  $d_n$  in the initial stages of the deposition also can be estimated from comparison of the curves. Figure 10 shows the correlation between  $k_{15}$  value and crystalline orientation of the film. FWHM values of  $\psi$ -scan and  $\phi$ -scan curve of the XRD (X-ray diffraction) pole figure show the degree of crystalline orientation in out-of plane and in-plane, respectively. Thicker films tend to have large  $k_{15}$  values even though they have same degree of crystalline orientation as thinner one. This kind of correlations and inhomogeneities characterization in wafer can be easily obtained from as-deposited film structure, by using present  $k$  value determination method.

#### 4.5 Conclusion

In this chapter, shear mode piezoelectric thin film resonators, which is promising for the acoustic microsensors operating in liquid, were introduced. Theoretical predictions of electromechanical coupling and tilt of wave displacement as functions of c-axis tilt angle showed that pure shear mode excitation by using c-axis parallel oriented wurtzite piezoelectric films expected to achieve high-Q and high-coupling sensor. Fabrication of c-axis parallel oriented films by ion beam orientation control technique and characterization of the film by a conversion loss of the as-deposited resonator structure were discussed.

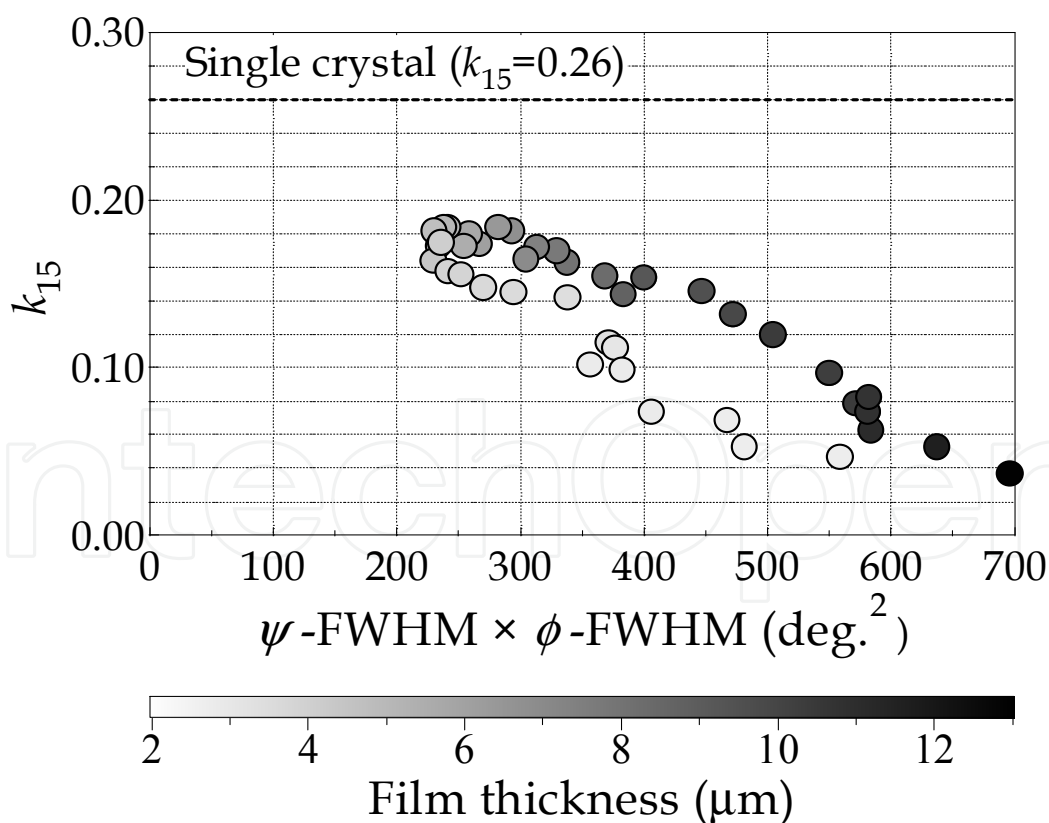


Fig. 10.  $k_{15}$  values of the ZnO piezoelectric layers as a function of multiplication of  $\psi$ -scan and  $\phi$ -scan profile curve FWHM values extracted from XRD pole figure (indicating the degree of crystalline orientation in out-of-plane and in-plane) (Yanagitani et al., 2007b)

## 5. References

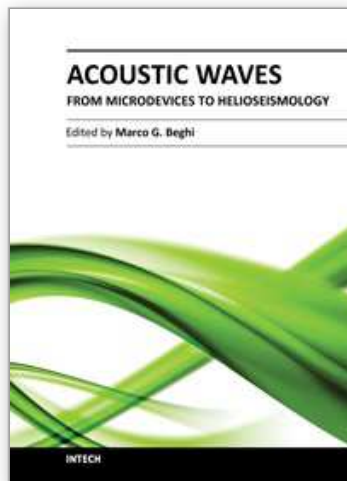
- Auld, B. A. *Acoustic Fields and Waves in Solid*. (1973). Vol. 1, pp. 73–76, A Wiley-Interscience Publication.
- Bond, W. (1943). The Mathematics of the Physical Properties of Crystals. *Bell System Technical Journal*, Vol. 22, pp. 1–72.
- Bradley R. M.; Harper J. M. E. & Smith, D. A. (1986). Theory of Thin-film Orientation by Ion bombardment during deposition. *J. Appl. Phys.*, Vol. 60, No. 12, pp. 4160–4164.
- Corso, C. D.; Dickherber, A. & Hunt, W. D. (2007). Lateral Field Excitation of Thickness Shear Mode Waves in a Thin Film ZnO Solidly Mounted Resonator. *J. Appl. Phys.* Vol. 101, pp. 054514-1-054514-7.
- Curie, P. (1885). *Bull. Soc. Franc. Miner. Crist.* Vol. 8 p. 145.
- Dobrev, D. (1982). Ion-beam-induced Texture Formation in Vacuum-condensed Thin Metal Films. *Thin Solid Films*, Vol. 92, No. 1-2, pp. 41–53.
- Dong, L. & Srolovitz, D. J. (1999). Mechanism of Texture Development in Ion-beam-assisted Deposition. *J. Appl. Phys. Lett.*, Vol. 75, No. 4, pp. 584–586.
- Dong, L.; Srolovitz, D. J.; Was, G. S.; Zhao, Q. & Rollett, A. D. (2001). Combined Out-of-plane and In-plane Texture Control in Thin Films using Ion Beam Assisted Deposition. *J. Mater. Res.*, Vol. 16, No. 1, pp. 210–216.
- Ensinger, W. (1995). On the Mechanism of Crystal Growth Orientation of Ion Beam Assisted Deposited Thin Films. *Nucl. Instrum. Meth. Phys. Res. B*, Vol. 106, pp. 142–146.
- Foster, N. F.; Coquin, G. A.; Rozgonyi, G. A. & Vannatta, F. A. (1968). Cadmium Sulphide and Zinc Oxide Thin-Film Transducers. *IEEE Trans. Sonic. Ultrason.*, Vol. 15, pp. 28–41.
- Fraser, D. B.; Krause, J. T. & Meitzler, A. H.; (1967). Physical Limitations on the Performance of Vitreous Silica in High-frequency Ultrasonic and Acousto-optical Devices. *Appl. Phys. Lett.* Vol. 11, No. 10, pp. 308–310.
- Fujimura, N.; Nishihara, T.; Goto, S.; Xu, J. & Ito, T. (1993). Control of Preferred Orientation for ZnOx Films: Control of Self-texture. *J. Crystal Growth*, Vol. 130, pp. 269–279.
- Harper, J. M. E.; Rodbell, K. P.; Colgan, E. G. & Hammond, R. H. (1997). Control of In-plane Texture of Body Centered Cubic Metal Thin Films. *J. Appl. Phys.* Vol. 82, pp. 4319–4326.
- Hickernell, F. S. (1996). Measurement Techniques for Evaluating Piezoelectric Thin Films. *Proc. IEEE Ultrason. Symp.*, pp. 235–242.
- Iijima, Y.; Tanabe, N.; Kohno, O. & Ikeno, Y. (1992). In-plane Aligned YBa<sub>2</sub>Cu<sub>3</sub>O<sub>7-x</sub> Thin Films Deposited on Polycrystalline Metallic Substrates. *Appl. Phys. Lett.*, Vol. 60, No. 6, pp. 769–771.
- Kaufman, D. Y.; DeLuca, P. M.; Tsai, T. & Barnett, S. A. (1999). High-rate Deposition of Biaxially Textured Yttria-stabilized zirconia by Dual Magnetron Oblique Sputtering. *J. Vac. Sci. Technol. A*, Vol. 17, pp. 2826–2829.
- Kawamoto, T.; Yanagitani T.; Matsukawa, M.; Watanabe, Y.; Mori, Y.; Sasaki, S. & Oba M. (2010). Large-Area Growth of In-Plane Oriented (11-20) ZnO Films by Linear Cathode Magnetron Sputtering. *Jpn. J. Appl. Phys.* Vol. 49 pp. 07HD16-1-07HD16-4.
- Kushibiki, J-I.; Akashi, N.; Sannomiya, T.; Chubachi, N.; & Dunn, F. (1995). VHF/UHF Range Bioultrasonic Spectroscopy System and Method. *IEEE Trans. Ultrason., Ferroelect., Freq. Contr.*, Vol. 42 No. 6, pp. 1028–1039

- Link, M.; Weber, J.; Schreiter, M.; Wersing, W.; Elmazria, O. & Alonot, P. (2007). Sensing Characteristic of High-frequency Shear Mode Resonators in Glycerol Solutions. *Sens. Actuators B*, Vol. 121, No.2, pp. 372–378.
- Matsumoto, Y.; Ujiie, T. & Kushibiki, J-I. (2000). Measurement of Shear Acoustic Properties of Water using the Ultrasonic Reflectance Method in Pulse-mode Operation. *Spring Meeting of Acoustical Society of Japan* (in Japanese)
- Meeker, T. R. (1996). IEEE Standard on Piezoelectricity (ANSI/IEEE Std. 176-1987). *IEEE Trans. Ultrason., Ferroelect., Freq. Contr.*, Vol. 43, No. 5, pp. 719–772..
- Milyutin, E. & Mural, P. (2010). Electro-Mechanical Coupling in Shear-Mode FBAR with Piezoelectric Modulated Thin Film. *IEEE Trans. Ultrason., Ferroelect., Freq. Contr.*, Vol. 58, No. 4, pp. 685–688.
- Milyutin, E.; Gentil, S. & Mural, P. (2008). Shear Mode Bulk Acoustic Wave Resonator Based on c-axis Oriented AlN Thin Film. *J. Appl. Phys.* Vol. 104, pp. 084508-1–084508-6.
- Mitsuyu, T.; Ono S. & Wasa, K. (1980). Structures and SAW Properties of Rf-sputtered Single-crystal Films of ZnO on Sapphire. *J. Appl. Phys.*, Vol. 51, No. 5, pp. 2464–2470.
- Naik, B. S.; Lutsky, J. J.; Rief R.; & Sodini, C. D. (1998). Electromechanical Coupling Constant Extraction of Thin-film Piezoelectric Materials Using a Bulk Acoustic Wave Resonator. *IEEE Trans. Ultrason., Ferroelect., Freq. Contr.*, Vol.45, No.1, pp. 257–263.
- Nakamura, K.; Shoji, T. & Kang, H. (2000). ZnO Film Growth on (01 $\bar{1}2$ ) LiTaO<sub>3</sub> by Electron Cyclotron Resonance-assisted Molecular Beam Epitaxy and Determination of Its Polarity. *Jpn. J. Appl. Phys.*, Vol. 39, No. 6A, pp. L534–L536.
- Ogi, H.; Hirao, M.; Honda T. & Fukuoka, H. (1995). Ultrasonic Diffraction from a Transducer with Arbitrary Geometry and Strength Distribution. *J. Acoust. Soc. Am.* Vol. 98, No. 2, pp. 1191–1198.
- Paco, P.; Menéndez, Ó. & Corrales E. (2008) Equivalent Circuit Modeling of Coupled Resonator Filters. *IEEE Trans. Ultrason., Ferroelect., Freq. Contr.*, Vol. 55, No. 9, pp. 2030–2037.
- Park, S. J.; Norton, D. P. & Selvamanickam, V. (2005). Ion-beam Texturing of Uniaxially Textured Ni Films. *Appl. Phys. Lett.*, Vol. 87, pp. 031907–031909.
- Ressler, K. G.; Sonnenberg, N. & Cima, M. J. (1997). Mechanism of Biaxial Alignment of Oxide Thin Films during Ion-Beam-Assisted Deposition. *J. Am. Ceram. Soc.*, Vol. 80, No. 10, pp. 2637–2648.
- Rosenbaum, J. F. (1988). Bulk Acoustic Waves: Theory and Devices. Artech House Boston London.
- Sauerbrey, G. (1959) Verwendung von Schwingquarzen zur Wägung Dünner Schichten und zur Mikrowägung. *Z. Physik*, Vol. 155, pp. 206–222.
- Smith, R. T. & Stubblefield, V. E. (1969). Temperature Dependence of the Electroacoustical Constants of Li-doped ZnO Single Crystals. *J. Acoust. Soc. Am.*, Vol. 46, pp. 105.
- Takayanagi, S.; Yanagitani, T.; Matsukawa, M. & Watanabe Y. (2010). A Simple Technique for Obtaining (11-20) or (10-10) Textured ZnO Films by RF Bias Sputtering," *Proc. 2010 IEEE Ultrason. Symp.* pp. 1060–1063.

- Van Wyk, G. N. & Smith, H. J. (1980). Crystalline Reorientation Due to Ion Bombardment. *Nucl. Instrum. Meth.*, Vol. 170, pp. 433–439.
- Weber, J.; Albers, W. M.; Tuppurainen, J.; Link, M.; Gabl, R.; Wersing, W. & Schreiter, M. (2006). Shear Mode FBARs as Highly Sensitive Liquid Biosensors. *Sens. Actuators A*, Vol. 128, No. 2, pp. 84–88.
- Wingqvist G.; Anderson H.; Lennartsson C.; Weissbach T.; Yantchev V. & Lloyd Spetz A. (2009). On the Applicability of High Frequency Acoustic Shear Mode Biosensing in View of Thickness Limitations Set by The Film Resonance. *Biosens. Bioelectron.*, Vol. 24 No. 11, pp. 3387–3390.
- Wingqvist, G. (2010). AlN-based Sputter-deposited Shear Mode Thin Film Bulk Acoustic Resonator (FBAR) for Biosensor Applications. *Surf. Coat. Tech.*, Vol. 205, No. 5, pp. 1279–1286
- Wingqvist, G.; Bjurström, J.; Liljeholm, L.; Yantchev, V. & Katardjiev, I. (2007). Shear mode AlN Thin Film Electro-acoustic Resonant Sensor Operation in Viscous Media. *Sens. Actuators B*, Vol. 123, No. 1, pp. 466–473.
- Wittstruck, R. H.; Tong, X.; Emanetoglu, N. W.; Wu, P.; Chen, Y.; Zhu, J.; Muthukumar, S.; Lu, Y.; & Ballato, A. (2003) Characteristic of  $Mg_xZn_{1-x}O$  Thin Film Bulk Acoustic Wave Devices. *IEEE Trans. Ultrason., Ferroelect., Freq. Contr.*, Vol. 50, pp. 1272–1277.
- Yanagitani, T. & Kiuchi, M. (2007c). Control of In-plane and Out-of-plane Texture in Shear Mode Piezoelectric ZnO Films by Ion-beam Irradiation. *J. Appl. Phys.*, Vol. 102, pp. 044115-1–044115-7.
- Yanagitani, T. & Kiuchi, M. (2007e). Highly Oriented ZnO Thin Films Deposited by Grazing Ion-beam Sputtering: Application to Acoustic Shear Wave Excitation in the GHz Range. *Jpn. J. Appl. Phys.* Vol. 46, pp. L1167–L1169.
- Yanagitani, T. & Kiuchi, M. (2011b). Texture Modification of Wurtzite Piezoelectric Films by Ion Beam Irradiation. *Surf. Coat. Technol.*, in press.
- Yanagitani, T., Matsukawa, M., Watanabe, Y., Otani, T. (2005). Formation of Uniaxially (11-20) Textured ZnO Films on Glass Substrates. *J. Cryst. Growth*, Vol. 276, No. 3-4, pp. 424-430.
- Yanagitani, T.; Arakawa, K.; Kano, K.; Teshigahara, A.; Akiyama, M. (2010). Giant Shear Mode Electromechanical Coupling Coefficient  $k_{15}$  in c-axis Tilted ScAlN Films. *Proc. 2010 IEEE Ultrason. Symp.*, pp. 2095–2098.
- Yanagitani, T.; Kiuchi, M.; Matsukawa, M. & Watanabe, Y. (2007b). Shear Mode Electromechanical Coupling Coefficient  $k_{15}$  and Crystallites Alignment of (11-20) Textured ZnO Films. *J. Appl. Phys.*, Vol. 102, pp. 024110-1–024110-7.
- Yanagitani, T.; Kiuchi, M.; Matsukawa, M. & Watanabe, Y. (2007d). Characteristics of Pure-shear Mode BAW Resonators Consisting of (11-20) Textured ZnO Films. *IEEE Trans. Ultrason., Ferroelect., Freq. Contr.*, Vol. 54, No. 8, pp. 1680–1686.
- Yanagitani, T.; Mishima, N.; Matsukawa, M. & Watanabe, Y. (2007a). Electromechanical Coupling Coefficient  $k_{15}$  of Polycrystalline ZnO Films with the c-axes Lie in the Substrate Plane. *IEEE Trans. Ultrason., Ferroelect., Freq. Contr.*, Vol. 54, No. 4, pp. 701–704.
- Yanagitani, T.; Morisato, N.; Takayanagi, S.; Matsukawa, M. & Watanabe, Y. (2011a) c-axis Zig-Zag ZnO Film Ultrasonic Transducers for Designing Longitudinal and Shear

- Wave Resonant Frequencies and Modes. *IEEE Trans. Ultrason., Ferroelect., Freq. Contr.*, Vol. 58, No. 5, pp. 1062–1068.
- Yu, L. S.; Harper, J. M. E.; Cuomo, J. J. & Smith, D. A. (1985). Alignment of Thin Films by Glancing Angle Ion Bombardment During Deposition. *Appl. Phys. Lett.*, Vol. 47, No. 9, pp. 932–933.
- Zhang, Y.; Wang Z. & Cheeke, J. D. N. (2003). Resonant Spectrum Method to Characterize Piezoelectric Films in Composite Resonators. *IEEE Trans. Ultrason., Ferroelect., Freq. Contr.*, Vol. 50, No. 3, pp. 321–333.

IntechOpen



## **Acoustic Waves - From Microdevices to Helioseismology**

Edited by Prof. Marco G. Beghi

ISBN 978-953-307-572-3

Hard cover, 652 pages

**Publisher** InTech

**Published online** 14, November, 2011

**Published in print edition** November, 2011

The concept of acoustic wave is a pervasive one, which emerges in any type of medium, from solids to plasmas, at length and time scales ranging from sub-micrometric layers in microdevices to seismic waves in the Sun's interior. This book presents several aspects of the active research ongoing in this field. Theoretical efforts are leading to a deeper understanding of phenomena, also in complicated environments like the solar surface boundary. Acoustic waves are a flexible probe to investigate the properties of very different systems, from thin inorganic layers to ripening cheese to biological systems. Acoustic waves are also a tool to manipulate matter, from the delicate evaporation of biomolecules to be analysed, to the phase transitions induced by intense shock waves. And a whole class of widespread microdevices, including filters and sensors, is based on the behaviour of acoustic waves propagating in thin layers. The search for better performances is driving to new materials for these devices, and to more refined tools for their analysis.

### **How to reference**

In order to correctly reference this scholarly work, feel free to copy and paste the following:

Takahiko Yanagitani (2011). Shear Mode Piezoelectric Thin Film Resonators, *Acoustic Waves - From Microdevices to Helioseismology*, Prof. Marco G. Beghi (Ed.), ISBN: 978-953-307-572-3, InTech, Available from: <http://www.intechopen.com/books/acoustic-waves-from-microdevices-to-helioseismology/shear-mode-piezoelectric-thin-film-resonators>

**INTECH**  
open science | open minds

### **InTech Europe**

University Campus STeP Ri  
Slavka Krautzeka 83/A  
51000 Rijeka, Croatia  
Phone: +385 (51) 770 447  
Fax: +385 (51) 686 166  
[www.intechopen.com](http://www.intechopen.com)

### **InTech China**

Unit 405, Office Block, Hotel Equatorial Shanghai  
No.65, Yan An Road (West), Shanghai, 200040, China  
中国上海市延安西路65号上海国际贵都大饭店办公楼405单元  
Phone: +86-21-62489820  
Fax: +86-21-62489821

© 2011 The Author(s). Licensee IntechOpen. This is an open access article distributed under the terms of the [Creative Commons Attribution 3.0 License](#), which permits unrestricted use, distribution, and reproduction in any medium, provided the original work is properly cited.

IntechOpen

IntechOpen